Table S1. Related to Figure 4

Statistics for EL_REC solution structure determination

Experimental restraints	
NOE Unambiguous restraints	2009
NOE Ambiguous restraints	710
Dihedral angle restraints	195
Hydrogen bond restraints	106
Mean rmsd from experimental restraints	
NOE, Å	0.03 ±0.001
Dihedral angles, °	0.2 ±0.06
Hydrogen bonds, Å	0.02 ±0.002
Average number of	
NOE violations > 0.5 Å	0
NOE violations > 0.3 Å	1.1 ±0.8
Dihedral violations > 5°	0
Hydrogen bond violations > 0.1 Å	0
Mean rmsd from idealized covalent geometry	
Bond lengths, Å	0.004 ±0.0001
Bond angles, °	0.49 ±0.01
Impropers, °	1.3 ±0.05
Geometric analysis of residues 144-257	
Rmsd from the mean	
Backbone atoms, Å	0.7 ±0.2
All heavy atoms, Å	1.3 ±0.2
Ramachandran analysis (PROCHECK)	
Most-favored regions, %	89.2 ±1.3
Allowed regions, %	9.8 ±1.6
Generously allowed regions, %	0.9 ±0.7
Disallowed regions, %	0.1 ±0.3

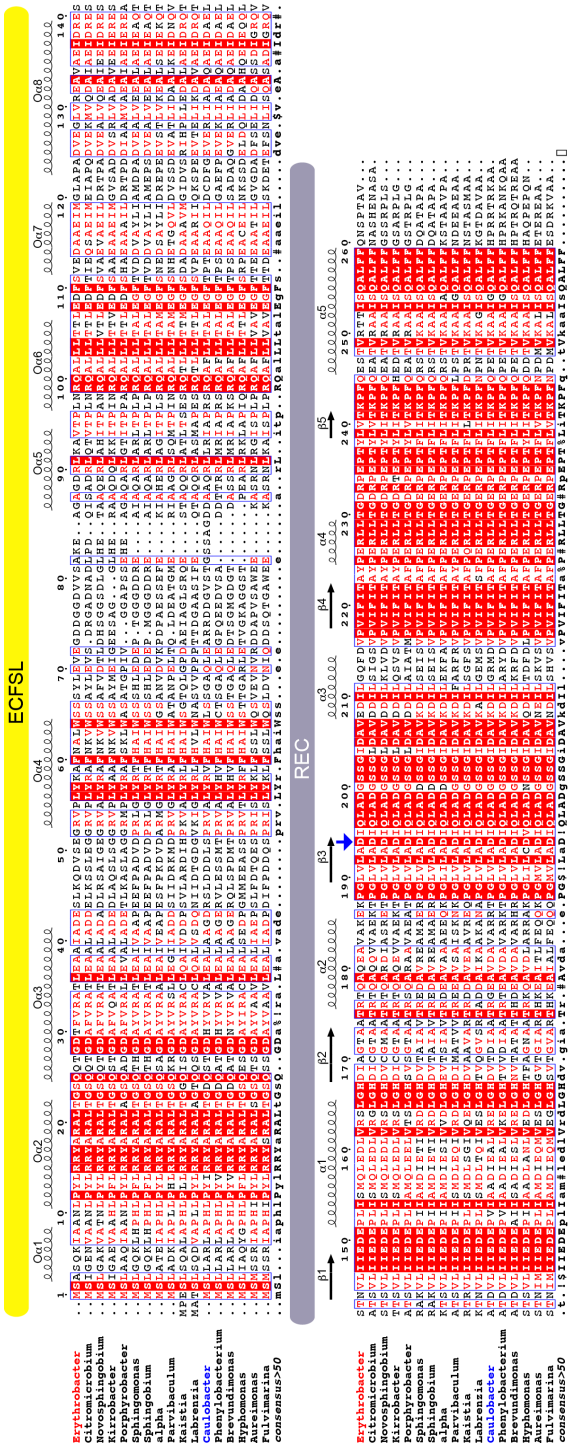

Figure S1. Related to Figure 1.

Sequence alignment of PhyR homologues, including *Erythrobacter litoralis* (red) and *Caulobacter crescentus* (blue). A blue arrow indicates the highly conserved phosphoacceptor aspartate. Other features indicated include the locations of the predicted secondary structures (subsequently confirmed by our structural studies), along with domain boundaries for the extracytoplasmic function sigma like domain (ECFSL, yellow) and receiver domain (REC, grey). Sequence alignment was performed using the program Multalin (http://multalin.toulouse.inra.fr/multalin) based on (Corpet, 1988).

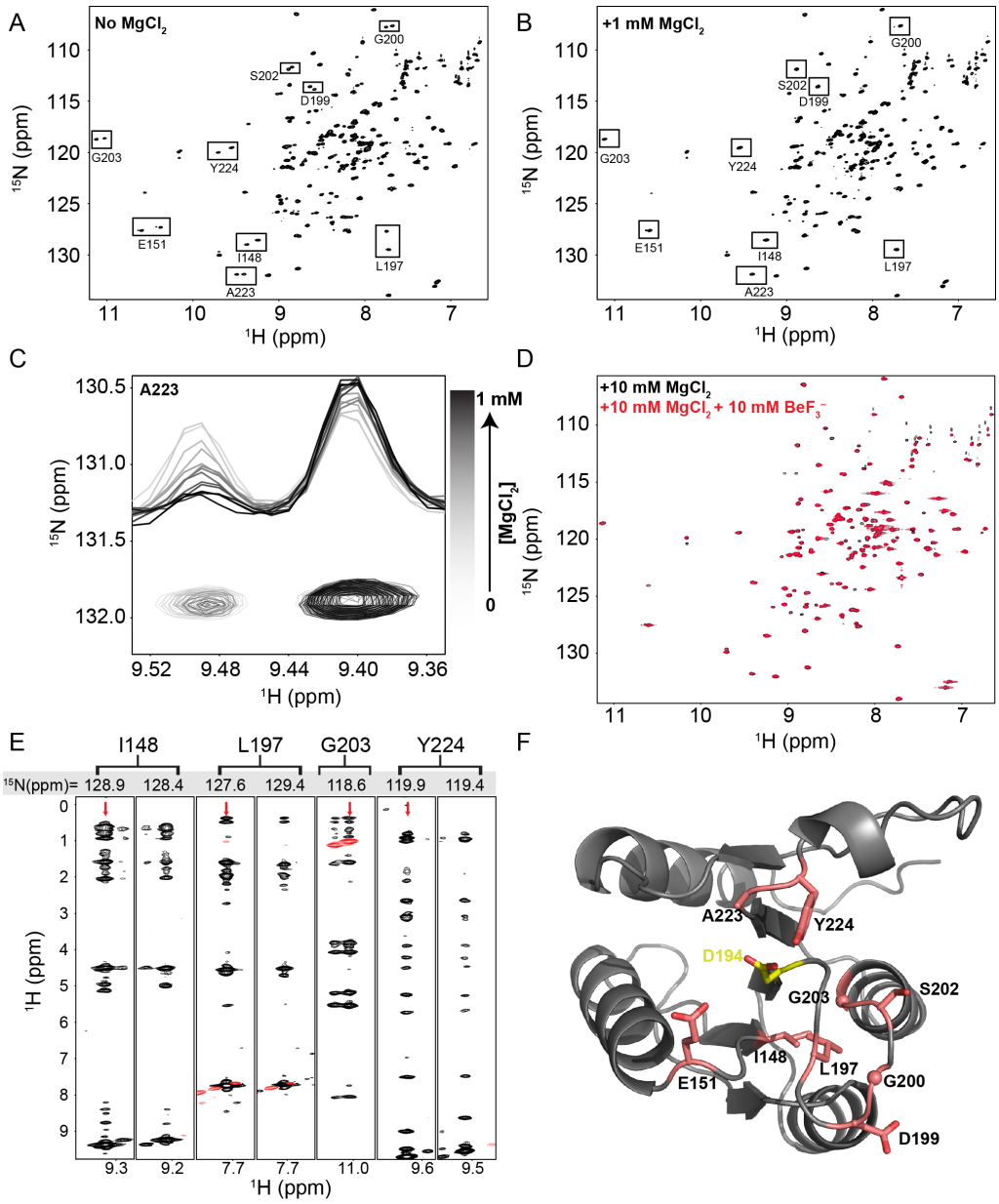

Figure S2. Related to Figures 2, 3 and 4

Binding of Mg^{2+} ions to EL_REC stabilizes a single protein conformation. (A) Removal of the ECFSL allows the REC domain to slowly interconvert between two conformations, as indicated by the appearance of multiple cross-peaks for several residues. Most of these resonances arise from residues associated with Mg^{2+} binding or adjacent to the metal binding site. Square boxes highlight examples of several cross-peaks showing such conformational exchange. (B) Addition of $MgCl_2$ reduced the number of doubled cross-peaks, demonstrating that divalent cation binding stabilizes one of the conformations. (C) As demonstrated by the A223 amide signal, titration with $MgCl_2$ changes the equilibrium between the two conformations, showing classic NMR slow exchange behavior. (D) Addition of BeF_3^- to Mg^{2+}-loaded EL_REC protein shows minor changes, consistent with the protein being in an active conformation. (E) Strips from ^{15}N-edited NOESY spectra show similar patterns of cross-peaks for both conformers, suggesting minimal structural differences between the two conformations. Red arrows indicate cross-peaks for dominant conformation (65% of sample); note that red peaks for G203 arise from spectral aliasing. (F) Residues undergoing this slow interconversion phenomenon (pink) map to a common regions on the EL_REC NMR structure, localized in loops near the active site (phosphoacceptor D194, yellow).

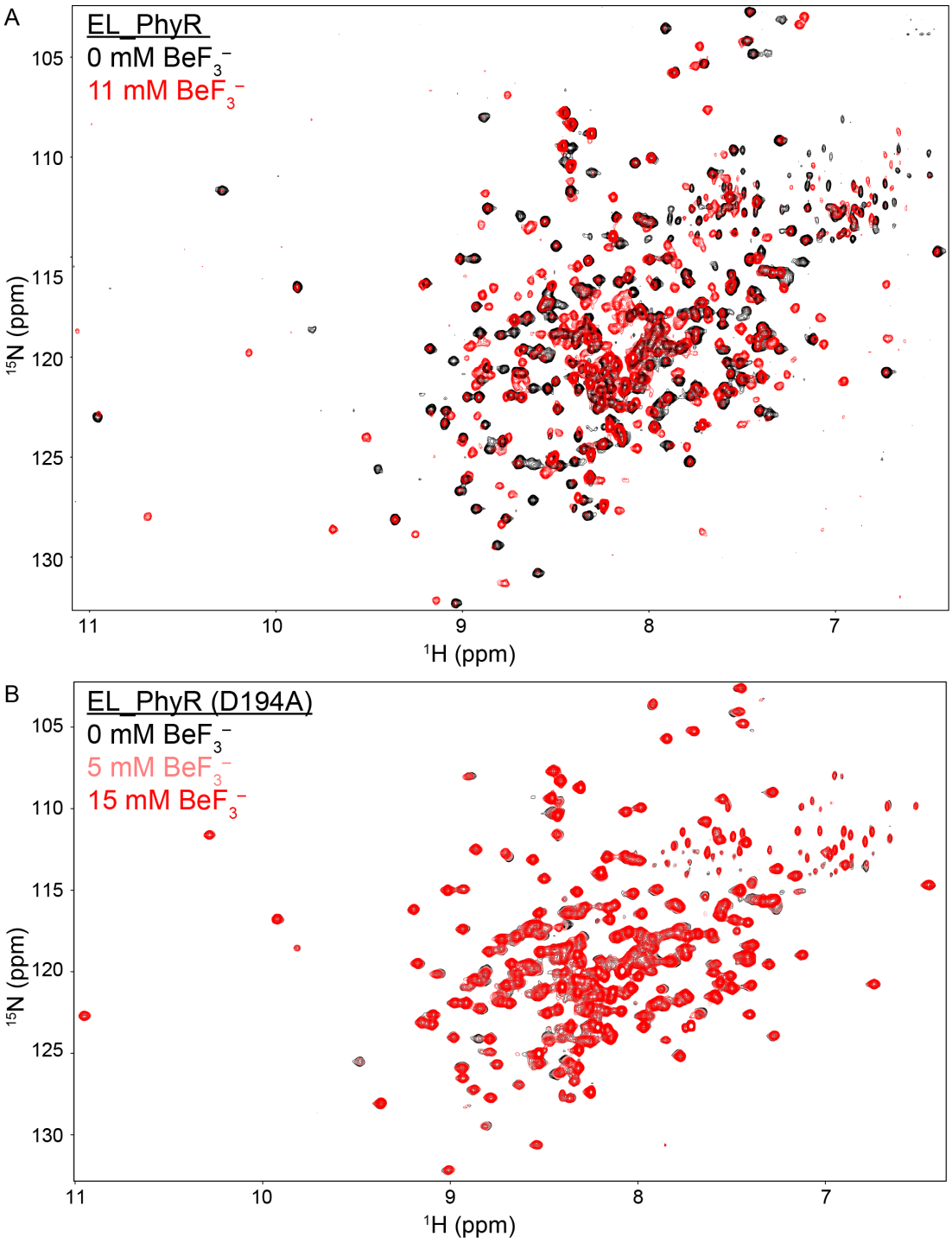

Figure S3. Related to Figures 2, 3, 5 and 7.

Mutation of the D194 phosphoacceptor residue disrupts BeF_3^- binding. (A) ^{15}N-^1H HSQC spectra of EL_PhyR in the presence and absence of BeF_3^- show extensive differences, indicating that BeF_3^- binding leads to marked changes on protein conformation. (B) In contrast, we observe very minor changes when BeF_3^- is added to EL_PhyR (D194A), confirming the critical role of this residue for phosphomimic binding. Buffer conditions: 20 mM HEPES (pH 7), 50 mM NaCl, 5 mM $MgCl_2$.

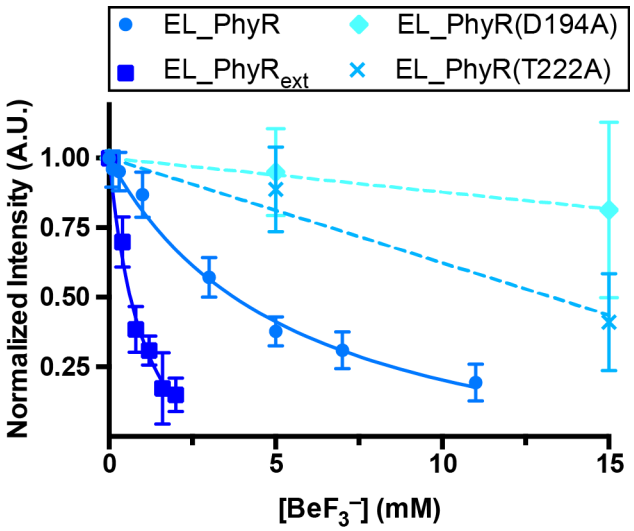

Figure S4. Related to Figures 2, 3, 5 and 7

EL_PhyR affinity for BeF_3^- can be modulated by mutations at or near the phosphoacceptor site, along with changes to the ECFSL-REC interdomain linker. Titration curves of EL_PhyR variants with BeF_3^- were obtained by monitoring changes in peak intensity in ^{15}N-^{1}H TROSY spectra; in each spectrum, normalized intensities of nine or ten probes were measured and averaged (error bars at ± one S.D.) for this analysis. Lines shown for EL_PhyR and EL_PhyR$_{ext}$ data correspond to fits to single site binding equations; dashed lines (D194A, T222A) are not fits and are included only for illustrative purposes. From these data, we see that extension of the interdomain linker by seven residues substantially increases BeF_3^- affinity consistent with biasing the REC domain into an active conformation (K_d: 1.0 mM for EL_PhyR$_{ext}$ *vs.* 5.5 mM for EL_PhyR). In contrast, D194A (diamond) and T222A (crosses) mutations reduce BeF_3^- binding affinity markedly. Buffer conditions: 20 mM HEPES pH 7, 50 mM NaCl, 5 mM $MgCl_2$.

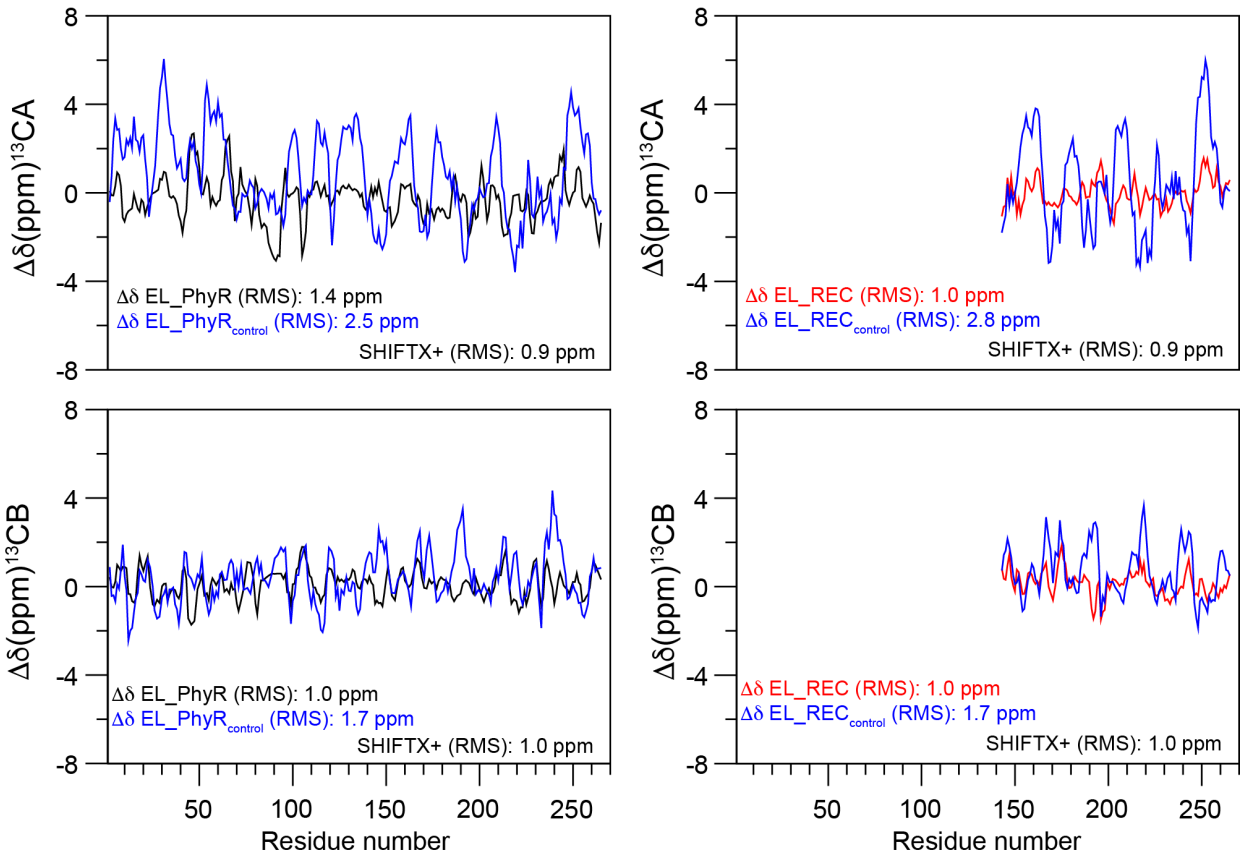

Figure S5. Related to Figure 4.

Chemical-shift based validation of the EL_PhyR homology model. Comparisons of experimental and calculated ^{13}CA and ^{13}CB chemical shifts were obtained by subtracting our experimental shifts from theoretical chemical shift assignments calculated by the program SHIFTX2 (Han et al., 2011):

$$\Delta\delta\ (\text{ppm}) = \delta(\text{SHIFTX2 calculated}) - \delta(\text{experimental})$$

Δδ values were calculated using the theoretical shifts of either our full-length protein homology model (EL_PhyR) or a representative member of the EL_REC NMR ensemble. To validate this approach, we also generated a pair of negative control data (EL_PhyR$_{control}$, EL_REC$_{control}$), which used SHIFTX2-based chemical shifts generated from artificially-extended versions of EL_PhyR and EL_REC proteins instead of the native structures. These negative controls should provide a calibration of Δδ values that would be obtained from highly incorrect structures.

Once calculated, we obtained RMS Δδ values prior to processing these parameters with a three-residue running average and plotting. Values approaching 0 indicate a better agreement between chemical shifts calculated by SHIFTX2 and experimentally-determined values.

These analyses reveal comparable RMS values among those generated from the EL_PhyR homology model, the experimentally-determined EL_REC structure, and the program's test set of 61 high-resolution X-ray structures (Han et al., 2011), providing independent verification of the quality of the EL_PhyR and EL_REC structures. Additionally, the substantial differences between Δδ EL_PhyR and Δδ EL_PhyR$_{control}$ (black and blue lines), with Δδ EL_PhyR closer to 0 provides further support our validation. Residue regions with higher chemical shift deviations between predicted and experimental chemical shifts (*e.g.* 40-50, 90-100) correspond to flexible loop regions that adopt different conformations as observed in the NMR structure of isolated ECFSL complexed with anti-σ (Campagne et al., 2012) and crystal structure of full-length PhyR (Herrou et al., 2010).

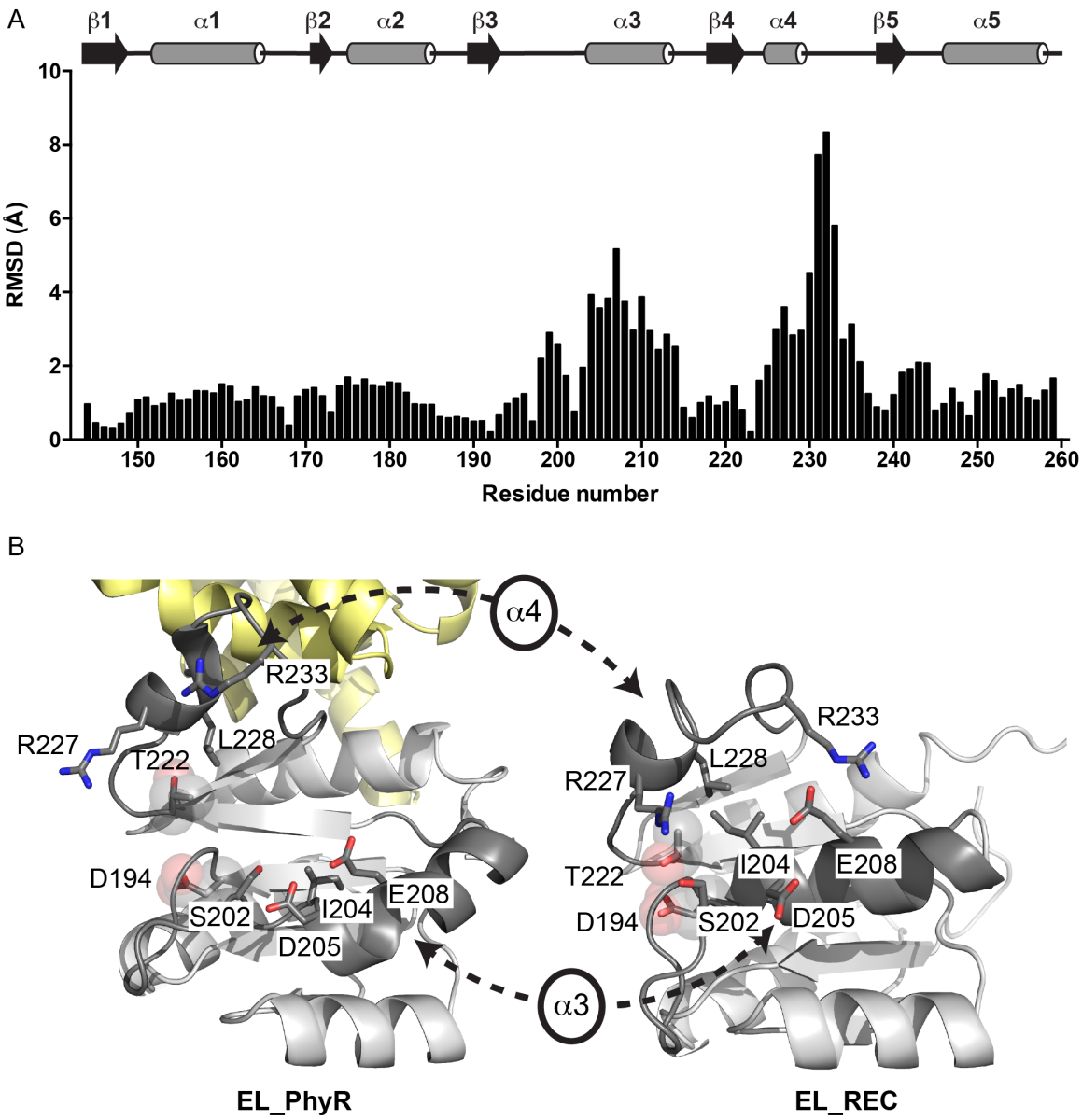

Figure S6. Related to Figures 4, 6 and 7.

Removal of the EL_PhyR ECFSL output domain substantially changes the α3-α4-β5 REC surface used for interdomain contact. (A) Comparison of backbone atom positions (N, CA, C, O) in the EL_PhyR homology model and EL_REC NMR structure were conducted by RMSD calculations. These demonstrate that largest changes are localized in the α4-β5 loop region, which directly contacts with the output domain in the full-length structure. Other regions with elevated RMSD values include the α3 helix, immediately adjacent to α4. Fitting was performed using the program ProFit (http://www.bioinf.org.uk/software/profit) based on (McLachlan, 1982). (B) The structural conformation of helices α3 and α4 in EL_REC are stabilized by a series of electrostatic (S202-R227, D205 and E208 with R233) and van-der-Waals (I204-L228) interactions.

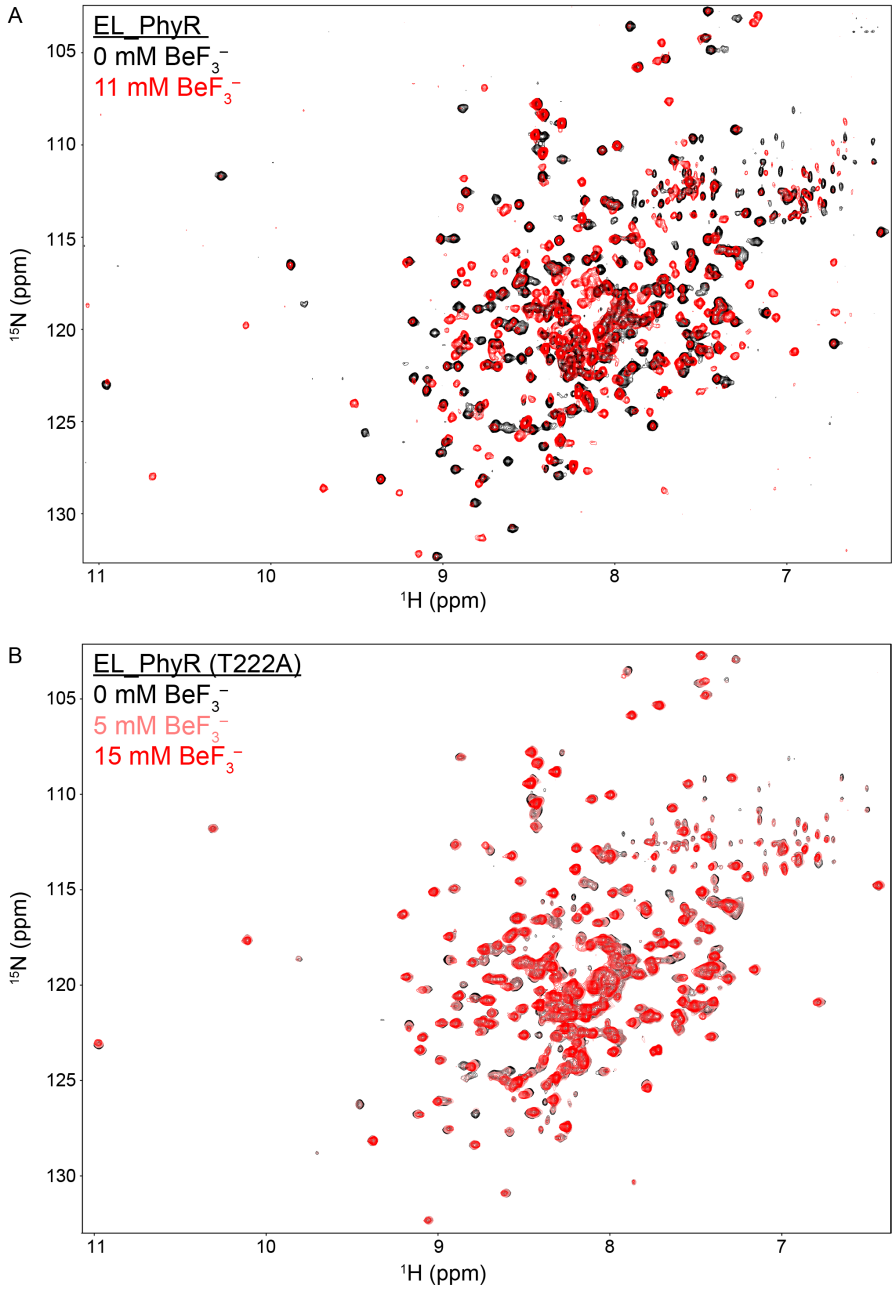

Figure S7. Related to Figures 2, 3, 5 and 7.

Threonine 222 plays an important role in PhyR activation. (A) ^{15}N-^{1}H HSQC spectra overlap of EL_PhyR in the presence and absence of BeF_3^- shows extensive differences, indicating that BeF_3^- binding leads to marked changes on protein conformation. *Note that this panel is a duplicate of Figure S3A, reprinted here to facilitate comparisons with the EL_PhyR (T222A) data presented below*. (B) In contrast, BeF_3^- titrations of the EL_PhyR (T222A) mutant show that the removal of interactions between Thr and nearby active site residues affected protein activation as indicated by the reduced spectral changes in contrast to wild-type (Panel A) with the addition of BeF_3^- up to 15 mM. Buffer conditions: 20 mM HEPES (pH 7), 50 mM NaCl, 5 mM $MgCl_2$.

Supplemental Experimental Procedures

Protein expression and purification

To express proteins in rich media, Escherichia coli BL21(DE3) cells were transformed with expression vectors and grown at 37 °C in LB media containing 100 μg/mL of ampicillin to an A_{600} of 0.8, then induced overnight at 18 °C by addition of 0.4 mM isopropyl β-D-thiogalactoside. Cells were harvested, resuspended into buffer with 50 mM Tris (pH 8), 100 mM NaCl.

To purify proteins, cells containing natural abundance or isotopically labeled (U-^{15}N, U-^{15}N/^{13}C, U-^{2}H/^{15}N/^{13}C) protein were lysed by extrusion, and centrifuged at 48,000 g for 45 min. The supernatant fraction was initially loaded onto a Ni^{2+} affinity column (Chelating Sepharose Fast Flow, GE Healthcare) pre-equilibrated with Tris (pH 8) and 100 mM NaCl plus 25 mM imidazole. Proteins were eluted using a 25 to 500 mM imidazole gradient and then digested with HIS6-TEV protease (Blommel and Fox, 2007). Cleaved target proteins were separated from their tags and TEV protease using a Ni^{2+} affinity column; flowthroughs were collected and concentrated (Amicon Ultra, Millipore). A final gel filtration step used HiLoad 16/60 Superdex 75, with column pre-equilibrated in 50 mM Tris at pH 8 and 100 mM NaCl buffer. All proteins were analyzed by SDS-PAGE and stored at 4 °C.

Phosphorylation assays

Samples of EL_PhyR (50 μM, either wild-type or T222A) were incubated with 5 μM of the EL368 histidine kinase (Correa et al., 2013) in 50 mM Tris (pH 8), 100 mM NaCl, 5 mM $MgCl_2$, 1 mM ATP and 12 μCi [γ-^{32}P] ATP (6000 Ci/mmol, Perkin Elmer) at room temperature. Aliquots were removed at intervals of 30, 45, 60, 75, 90, 120 and 150 s, then quenched into 4 x SDS-PAGE sample buffer (50 mM Tris (pH 6.8), 200 mM NaCl, 40 mM EDTA, 0.2% bromophenol blue, 10% (v/v) β-mercaptoethanol, 4% (w/v) SDS, and 20% (v/v) glycerol). After electrophoresis, the dye front and unincorporated ATP were removed with a razor blade. Subsequently, gels were dried under vacuum at 80 °C for 45 min and exposed for 30 to 60 min to a phosphoimager screen that was later scanned with a Fujifilm FLA-5100.

Supplemental References

Blommel, P.G., and Fox, B.G. (2007). A combined approach to improving large-scale production of tobacco etch virus protease. Protein Expr Purif *55*, 53-68.

Campagne, S., Damberger, F.F., Kaczmarczyk, A., Francez-Charlot, A., Allain, F.H., and Vorholt, J.A. (2012). Structural basis for sigma factor mimicry in the general stress response of Alphaproteobacteria. Proc Natl Acad Sci U S A *109*, E1405-1414.

Corpet, F. (1988). Multiple sequence alignment with hierarchical clustering. Nucleic Acids Res *16*, 10881-10890.

Correa, F., Ko, W.H., Ocasio, V., Bogomolni, R.A., and Gardner, K.H. (2013). Blue Light Regulated Two-Component Systems: Enzymatic and Functional Analyses of Light-Oxygen-Voltage (LOV)-Histidine Kinases and Downstream Response Regulators. Biochemistry *52*, 4656-4666.

Han, B., Liu, Y., Ginzinger, S.W., and Wishart, D.S. (2011). SHIFTX2: significantly improved protein chemical shift prediction. J Biomol NMR *50*, 43-57.

Herrou, J., Foreman, R., Fiebig, A., and Crosson, S. (2010). A structural model of anti-anti-sigma inhibition by a two-component receiver domain: the PhyR stress response regulator. Mol Microbiol *78*, 290-304.

McLachlan, A.D. (1982). Rapid comparison of protein structures. Acta Cryst *A38*, 871-873.